RESEARCH ARTICLE

Quantum Crystallography and Complementary Bonding Analysis of Agostic Interactions in Titanium Amides

Lorraine A. Malaspina,[a] Nils Frerichs,[b] Christian Adler,[b] Marc Schmidtmann,[b] Rüdiger Beckhaus,*[b] and Simon Grabowsky*[a]

[a] Departement für Chemie, Biochemie und Pharmazie, Universität Bern, Freiestrasse 3, CH-3012 Bern, Switzerland, e-mail: simon.grabowsky@unibe.ch
[b] Institut für Chemie, Carl von Ossietzky Universität Oldenburg, Carl-von-Ossietzky-Straße 9–11, DE-26129 Oldenburg, Germany, e-mail: ruediger.beckhaus@uni-oldenburg.de

In memory of Professor *Jack D. Dunitz*

Agostic interactions involving titanium are textbook examples for C–H bond activation. Therefore, it is surprising that there is no study in the literature in which the hydrogen atom in the C–H···Ti interaction has been determined reliably, although nearly all the criteria for assessing the strength and character of the agostic interaction depend on the hydrogen atom and its position. Here, we demonstrate with quantum crystallographic techniques how hydrogen atoms in a series of three titanium amides can indeed be localized accurately and precisely based on routine single-crystal X-ray diffraction data. Once the hydrogen positions have been established, theoretical and experimentally fitted bonding analyses reveal that the C–H···Ti interaction becomes stronger with increasing inter-ligand London dispersion stabilization of bulky alkyl groups.

Keywords: agostic interactions, C–H activation, complementary bonding analysis, quantum crystallography, titanium, titanium amides.

Introduction

Agostic interactions activate C–H bonds and hence play a key role in organometallic transformations and catalytic processes.[1–4] They are defined as partially covalent 2-electron-3-center C–H···metal interactions.[5] They are especially prominent with early transition metals because the bonding can be understood as a partial charge transfer from a C–H bond to vacant d-orbitals at the metal; and here compounds with agostic interactions involving the light d^0 Ti ion are the seminal and textbook examples.[6–13] Among them, titanium amides are relevant for synthetic procedures,[14,15] are reasonably accessible with a variety of ligand systems,[16] and have been used as

model systems to understand the bonding nature of agostic interactions as such.[10,17] For these reasons, we have here selected a series of three related titanium amides with varying bulkiness of the ligands at the Ti-atom (*Figure 1*) to study the role and impact of the hydrogen atom on the agostic bond with experimental techniques from quantum crystallography.

Some of the most commonly used criteria for the identification and characterization of the agostic bond involve: 1) *geometry*, elongation of the C–H bond, relatively short H···M distances (1.8–2.3 Å), small C–H···M angles (90–140°) and increasing C···M···H angles;[18] 2) *IR vibrational spectroscopy*, a red shift of the C–H stretching vibration[19] related to the C–H bond elongation/weakening and larger values of the C–H compliance constant;[20] 3) *^{1}H-NMR spectroscopy*, low $^1J_{CH}$ value (50 to 100 Hz) and an upfield shift δ_H relative to an uncoordinated CH group;[18,21] 4) *electron density*, a quantum theory of atoms in molecules
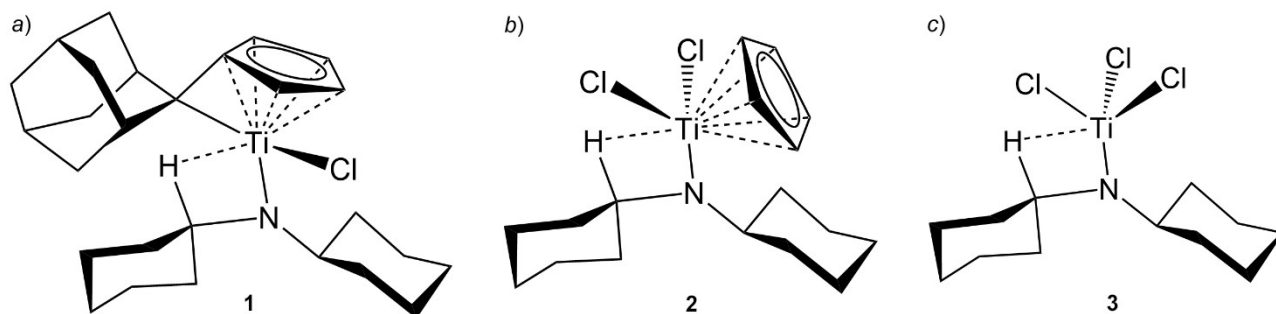
Figure 1. Titanium amide compounds with agostic interactions used in this study with decreasing bulkiness of ligands at the Ti-atom. *a*) Compound **1** (ref.[16]), *b*) compound **2** (this study), *c*) compound **3** (ref.[16]).

(QTAIM[22]) topological electron-density pattern indicating the presence of a M···H interaction[23] as well as a region of local charge depletion at the metal ion core;[24,25] *5*) *bonding descriptors* based on natural bond orbitals (NBO[26]), electron localization and localizability functions (ELF,[27] ELI[28]) or the non-covalent interaction (NCI[29]) index.[30–33]

From an experimental point of view, there are two major problems or challenges related to the above criteria: *1*) All criteria depend critically on the hydrogen atom; and for all but the spectroscopic criteria, no reliable statement can be made without an accurate and precise localization of the hydrogen atom in the agostic bond from diffraction experiments. *2*) Electron-density related criteria of agostic interactions can be assessed through modelling of the experimental charge density based on high-resolution, low-temperature single-crystal X-ray diffraction experiments.[12,13,34] But all other bonding descriptors are based on orbitals or the density matrix and are therefore not accessible through experimental electron-density determination.

Localization of Hydrogen Atoms in Agostic Bonds

The most accurate and precise way of experimentally determining hydrogen atom positions is neutron diffraction. In the Cambridge Structural Database (CSD), there is a total of 46 entries of compounds with Ti-involving agostic interactions, but not even one of them has been determined by neutron diffraction.[35] Hence, there are no experimental reference values for distances or angles in C–H···Ti agostic interactions. The average alkylic C–H bond distance not involved in an interaction is between 1.077 and 1.099 Å averaged over a few thousand neutron diffraction studies of organic and organometallic compounds.[36] For covalent terminal Ti–H bonds, there is not a single neutron

diffraction study in the CSD either. The distance is estimated to be around 1.75 Å in $Cp*_2TiH$[37] and $CpTi(CO)_2(Me_2PCH_2CH_2PMe_2)H$.[38] There is one neutron diffraction study of a compound with a hydrogen atom bridging B- and Ti-atoms with a Ti–H distance of 1.904(15) Å.[39]

Consequently, none of the 46 studies of C–H···Ti interactions found in the CSD includes reliable experimental information on the hydrogen atom position. In the most common case, free refinements of the H-atom positions in the independent atom model (IAM) have been undertaken. The results are imprecise and always too short. In 28 cases, the distances are below 1.00 Å, ranging from 0.80(6) to 0.99(4) Å. In only eight cases are the C–H distances between 1.00 and 1.10 Å, although we recall from the previous paragraph that an unperturbed C–H distance is in the range of 1.077 and 1.099 Å, so an agostic one should be significantly longer. We have summarized and cited these 36 cases in *Table S1* in the *Supporting Information*. In all other cases but three (see below), the hydrogen atom position was not refined (mostly as a relic of the riding model applied in automated or routine Shelx IAM refinements[40]) or information was not available. In one particular study,[41] good data quality and an extremely close and linear C–H–Ti approach led to IAM-refined values of C–H = 1.19(2) and Ti–H = 1.66(2) Å. If a multipole model is used instead of IAM, free refinement of H-atom positions works more reliably (for a C–H···Ni interaction 'we could freely refine the respective C_β–H_β bond distance of 1.20(1) Å, in good agreement with the DFT calculations [1.205 Å]'[34]). Alternatively, in multipole models of compounds with C–H···Ti interactions, C–H distances are fixed to those from theoretical geometry optimization.[12,25]

More recently, *Hirshfeld* Atom Refinement (HAR) of X-ray diffraction data has shown to reliably determine

X—H distances in organic compounds as precisely and as accurately as it is possible with neutron diffraction data,[42] avoiding all the workarounds summarized in the previous paragraph. This is possible because in HAR the non-spherical electron-density distribution is taken into account which is especially impactful for the treatment of hydrogen atoms that only have a valence electron participating in bonding and no spherical core electron density distribution.[43–45] These advantages are currently attempted to be transported to transition metal hydrides.[46,47] Therefore, there have been first reports in which unusual agostic-type bonding situations were tackled with HAR: a reverse agostic Rh—H···Si interaction,[48] and a C—H···Rb interaction.[49] Here, we will apply and test HAR more systematically to the textbook C—H···Ti agostic interactions.

Complementary Bonding Analysis with X-Ray Fitted Wavefunctions

As an alternative to electron-density modelling using the multipole *pseudo*-atom formalism,[50] X-ray constrained wavefunction (XCW) fitting also describes the redistribution of electron density due to bonding and non-bonding effects based on the measured X-ray structure factors.[51–54] The advantage, however, is that not only the average electron density is available after the XCW fitting, but the full density matrix, so that in addition to QTAIM all such bonding descriptors based on NBO, ELF, ELI, NCI index *etc.* are available that belong to a balanced complementary bonding analysis.[55] Hence, we show how the effect of XCW fitting impacts on the comparatively weak agostic interactions in comparison to purely theoretical reference calculations. For a full NBO analysis including E(2) perturbation energies, we had to write and implement a new script that reads the Fock matrix after XCW fitting, modifies it and transfers it to the NBO software. Unfortunately, an XCW-based compliance matrix analysis was not feasible because it depends on the Hessian matrix which requires a frequency analysis that is not available after XCW for technical reasons.

The measured X-ray structure factors of compounds **1** to **3** were always treated with a protocol of subsequent HAR and XCW fitting. This procedure is termed X-ray wavefunction refinement (XWR) and relies on the interplay between accurate geometrical refinement based on fixed theoretical wavefunctions (HAR) and modification of the molecular orbitals based on fixed HAR-derived geometries (XCW fitting).[56] These two steps are strictly separated to avoid

parameter correlation and overfitting but include the effect of thermal motion also in the wavefunction fitting part. More details are described in the review ref.[53]. XWR is the most advanced technique available today for the analysis of single-crystal X-ray diffraction data, and therefore we believe that it is this method applied to weak bonding interactions that deserves to be showcased in the framework of a special issue honoring the pioneer of small-molecule single-crystal crystallography *Jack Dunitz*, a sceptic of weak atom-atom bonds.[57,58]

Results and Discussion

Crystal Structures and Geometry

The molecular geometries of **1**–**3** after HAR are shown in *Figure 2*. All atom coordinates and atomic displacement parameters (ADPs) were freely refined, including those for hydrogen atoms. All hydrogen ADPs are physically reasonable. The main axes of vibration in **1** and **3** are clearly oriented in the direction of the Ti bonding partner, in **2** less clearly. These geometries are the basis for all further analyses below.

In *Figure 3*, C—H involving bond distances and C—H···Ti angles are plotted with their standard uncertainties in different refinement models for the X-ray data (IAM *vs.* HAR) compared to values from neutron diffraction and from theory. It is obvious that the results from IAM are inaccurate and imprecise; the C—H bond distances are far too short, and the angles far too wide compared to the reference values (measure of accuracy) as well as the error bars much longer than for HAR, especially for the C—H···Ti angles (measure of precision). This showcases how inadequate any discussion of geometrical parameters involving hydrogen atoms is if neither neutron-diffraction derived nor HAR-derived values are used. A slight elongation of the agostic C—H bond relative to the averaged unperturbed values from neutron diffraction and to the averaged non-agostic C—H bonds in the cyclohexyl ligands in **1** to **3** from HAR is visible, just outside the standard uncertainties in **1** and **3**, but inside the standard uncertainty in **2**. These differences are discussed below in more detail in reference to *Table 1*. The theoretical values do not reflect this elongation as accurately as the HAR-derived results. Concerning the C—H···Ti bond angles, they are much closer to 90° in **3** than in **1** and **2**, which is discussed in more detail below with respect to *Table 2*.

Table 1 shows the absolute values with their standard deviations (sds) for the C—H bonds in differ-
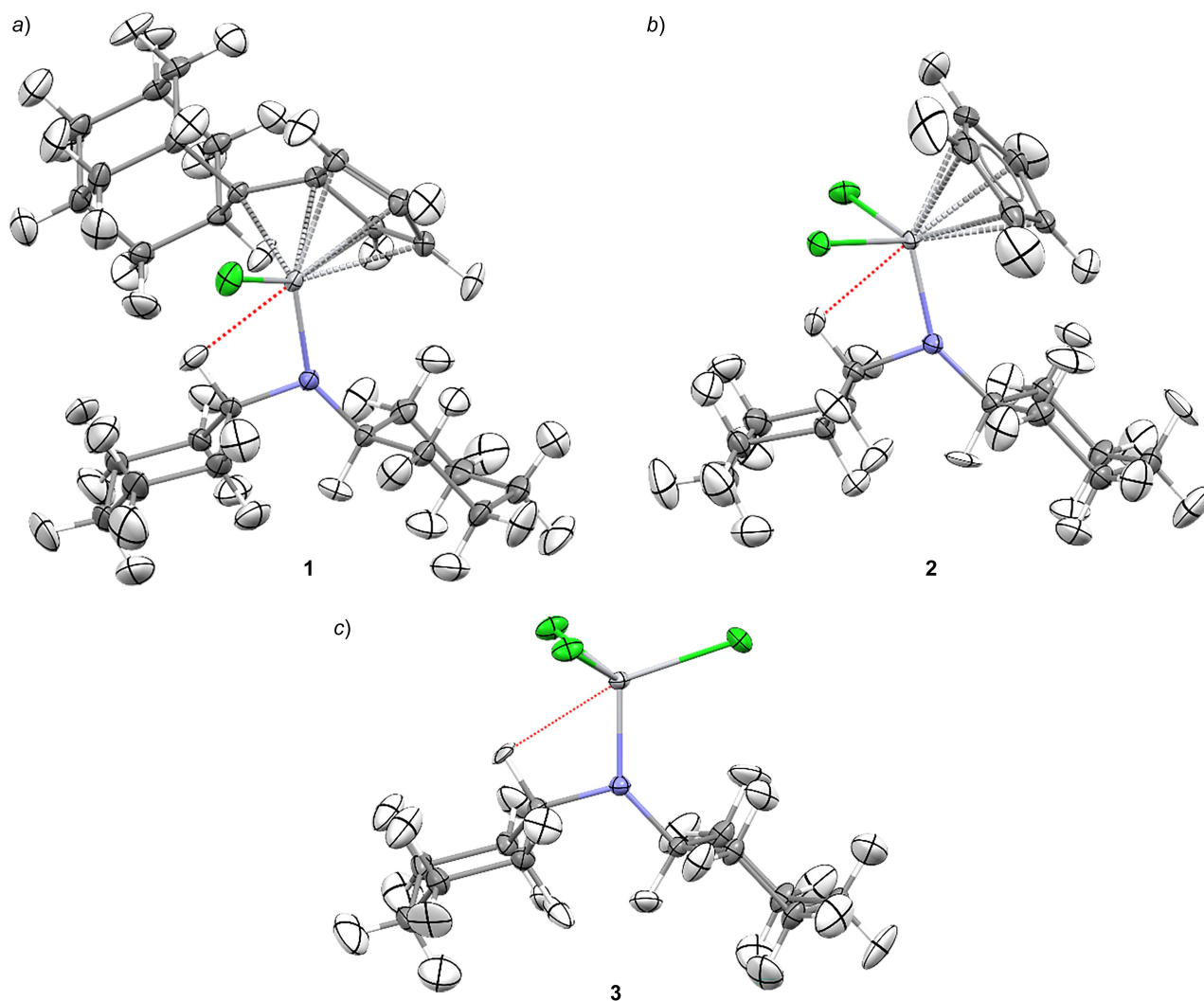
Figure 2. Final geometries after HAR for compounds *a*) **1**, *b*) **2**, *c*) **3**. All atoms, including hydrogen atoms, were freely and anisotropically refined. Atomic displacement parameters (ADPs) at 50% probability level. The agostic interactions are highlighted by red dotted lines. Light grey = Ti, dark grey = C, white = H, blue = N, green = Cl.

ent models or from different techniques. To estimate how reliable the HAR-derived C–H bonds lengths are, the average results from *Allen* and *Bruno* for methylene groups are compared to the average bond lengths obtained from HAR for the cyclohexyl groups in **1** to **3**. For **2**, the values match perfectly, whereas for **1** and **3** the differences are as small as 0.009 and 0.006 Å. This difference is half or a third of the sds, so we consider the HAR results to be reliable and physically meaningful. In this context, the HAR-derived bond distance of the agostic C–H bond compared to the entry *neutron (av.)* (H-atom at a tertiary carbon atom with at least one hetero atom such as nitrogen as next neighbor) shows a clear elongation. The agostic C–H bond is longer by more than one sd for **1**

and **3**, and longer but within one sd for **2**. In any case, this is a measure of the weakening of the C–H bond due to the interaction with the Ti-atom. Interestingly, the optimized geometries (last entry in *Table 1* and *Table S3* in the *Supporting Information*) contain consistently shorter C–H bonds with only a very small elongation relative to the values from neutron diffraction.

The Ti···H separations and C–H···Ti angles are given in *Table 2*. According to the criteria summarized in *Brookhart*, *Green* and *Parkin*,[18] they are at the upper limit of agostic interactions (1.8–2.3 Å). The C–H···Ti angles are at the lower limit around 90° (range 90–140°). *Table S4* in the *Supporting Information* shows that if the same C–H bond is not involved in an
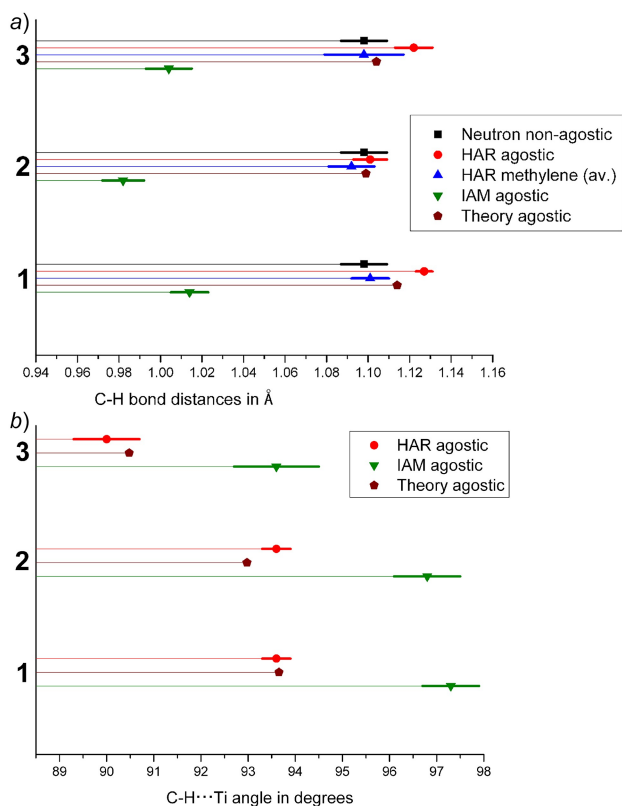
a)

b)

Figure 3. *a*) IAM, HAR, neutron and theory-derived C–H bond lengths for **1**–**3**. Theory=**M+D+Emp** (see *Computational Part* for the definition of the theoretical models). 'Neutron non-agostic' are averaged C–H distances referring to the standard values from neutron diffraction by Allen and Bruno.[36] 'HAR methylene (av.)' refers to all remaining HAR-refined methylene C–H bonds in the cyclohexyl groups of **1**–**3** that are not involved in the agostic interaction. The error bars refer to sample standard deviations for all averaged values, whereas for all individual IAM and HAR values they are estimated from the variance-covariance matrix upon refinement. The error bars can be regarded as a measure of precision. *b*) IAM, HAR, and theory-derived C–H···Ti angles involving the agostic H-atom. The errors bars are estimated standard uncertainties from the refinements.

agostic interaction, it becomes necessarily larger by geometric considerations and the C···Ti···H angle more acute (*Table S5*). If the C–H···Ti angle is about 90°, then an elongation of the C–H bond leads to a shortening of the Ti···H distance, see insert picture in *Table 2*. This is reflected here in the fact that the geometry-optimized Ti···H distances are always longer than the HAR-derived ones as the optimized C–H distances are much shorter (see previous paragraph and *Table 1*), and in addition the optimized C–H···Ti angles are slightly larger than the experimental ones, however, only by a maximum of about 0.5°. Relative to the isolated-molecule model **G**, the inclusion of both

Table 1. X–H bond lengths (in Å) derived for HAR compared to neutron diffraction average values from *Allen* and *Bruno* (*neutron (av.)*).[36] *HAR methylene (av.)* refers to all remaining HAR-refined methylene C–H bonds in the cyclohexyl groups of **1**–**3** that are not involved in the agostic interaction. The values in brackets are sample standard deviations for all averaged values, whereas for all individual IAM and HAR values they are estimated standard uncertainties from the variance-covariance matrix upon refinement. The C–H distance from theoretical geometry optimization is given at the highest level **M+D +Emp**, whereas the theoretical values from all other models are given in Table S3 in the Supporting Information. See the *Computational Part* for the definition of the theoretical models.

	1	**2**	**3**
neutron (av.)	1.098(11)	1.098(11)	1.098(11)
neutron methylene (av.)	1.092(17)	1.092(17)	1.092(17)
HAR methylene (av.)	1.101(9)	1.092(11)	1.098(19)
HAR agostic	1.127(4)	1.102(8)	1.122(9)
M+D+Emp	1.112	1.100	1.105

empirical dispersion correction and a simulation of the environment brings the optimized geometries closer to the experimental ones in that the Ti···H separation shortens. For the C–H···Ti angles, the effect of the environment is not visible, but the use of empirical dispersion corrections does reduce the angles to make them more similar to the experiment. Overall, no clear improvement of the use of dipoles in addition to monopoles can be seen. Therefore, the model **M+ Emp** will be used in the complementary bonding analysis section below.

The *Hirshfeld* surfaces[60] and fingerprint plots[61] in *Figure 4* are a different representation of geometrical proximity. Only the amide ligand *Hirshfeld* surface (HS) is plotted and transformed into the fingerprint plot. Since the N–Ti bond has been cut in this approach, there is an intense red region signaling geometric proximity in this area, generating the long spike in the fingerprint plot in the grey area. However, the contact area on the HS is not circular, only on the right-hand side. On the left, it is deformed in all three cases due to the presence of a secondary interaction between the Ti-atom and the ligand, namely the agostic C–H···Ti interaction. The small red arrow points from the Ti-atom to the H-atom mediated by the HS. The total H···Ti contact area is also depicted in blue on the fingerprint plot and the closest of these contact points leads to an imprint that represents the fingerprinting of the agostic interaction. We believe that the unprecedented procedure described here, namely plotting the ligand HS and searching for a fingerprint of the agostic interaction, is simple and quick, because

Table 2. Ti···H distances (in Å) and C–H···Ti angles (in °) across all theoretical models and the HAR refinements. The sum of the *van-der-Waals radii* of Ti and H is 3.47 Å.[59]
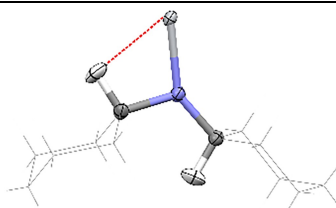
Model	1		2		3	
G	2.309	93.81	2.345	93.96	2.442	90.43
M	2.279	94.18	2.353	93.98	2.419	90.60
M+D	2.319	93.69	2.356	93.75	2.414	90.53
G+Emp	2.267	93.58	2.294	93.93	2.406	90.30
M+Emp	2.260	93.65	2.298	93.98	2.382	90.48
M+D+Emp	2.273	93.59	2.305	93.69	2.378	90.39
HAR	2.252(4)	93.6(3)	2.258(9)	93.6(5)	2.368(13)	90.0(6)

only based on geometric proximity, and should be tested for the identification of different agostic interactions in future studies.

Complementary Bonding Analysis

The following bonding analyses were carried out only for the theoretical model **M+Emp** (simply abbreviated *theory* in the following, see *Computational Part* for the definition of the theoretical models) since the geometrical results discussed above are similar to those derived from the highest model **M+D+Emp** and since **M+Emp** gave less technical and convergence problems in the bonding analysis software programs. All the same analyses were carried out for the fitted wavefunctions after the full X-ray wavefunction refinement (XWR) protocol. However, only the compliance matrix analysis and the second order perturbation theory in NBO are exceptions in that the results from theory are compared to the results from singlepoint (SP) calculations at the fixed HAR geometries (see *Computational Part*).

Table 3 summarizes the results of the compliance matrix analysis. Larger values of the compliance constant mean weakening of a bond.[62] Without exception, the values for the C–H bonds that are involved in the interaction with the Ti-atom are higher by between about 0.01 and 0.04 Å mdyn^{-1} than the ones for the unperturbed reference C–H bonds. This confirms a measurable weakening of the bonds and hence an identification of the agostic interactions. The effect is more pronounced at the HAR geometries than at the optimized geometries in agreement with a

Table 3. Compliance constants from compliance matrix analysis for two different C–H bonds, one involved and one not involved in the agostic C–H···Ti interaction. Values are given in Å mdyn^{-1}. The non-agostic C–H bond considered is the one highlighted in the insert graphic in Table 2.

	1	2	3
Theory			
agostic C–H	0.235	0.212	0.222
non-agostic C–H	0.207	0.203	0.200
SP at HAR geometry			
agostic C–H	0.245	0.220	0.231
non-agostic C–H	0.207	0.205	0.195

larger bond elongation in HAR relative to theory (see *Table 1* for comparison).

To get a more global view of the intramolecular interactions present in compounds **1** to **3**, *Figure 5* shows the NCI index plotted as colored isosurfaces of the reduced density gradient. Red means repulsion, blue means electrostatic attraction and green/brown refers to weakly attractive *van-der-Waals* interactions. There is no principle difference between the NCI plots from theory and XWR, so the conclusions hold in either model. In all models and for all compounds, the C–H···Ti interaction has diffuse regions of weakly attractive, but also, towards the Ti-atom, areas of weakly repulsive forces that normally occur in regions of steric crowding (for example inside the cyclohexyl- and adamantyl rings/cages). This means that the approach of the C–H bond to the Ti-atom, which is far below the sum of the individual *van-der-Waals* radii (see *Table 2*), gives rise to both attraction through
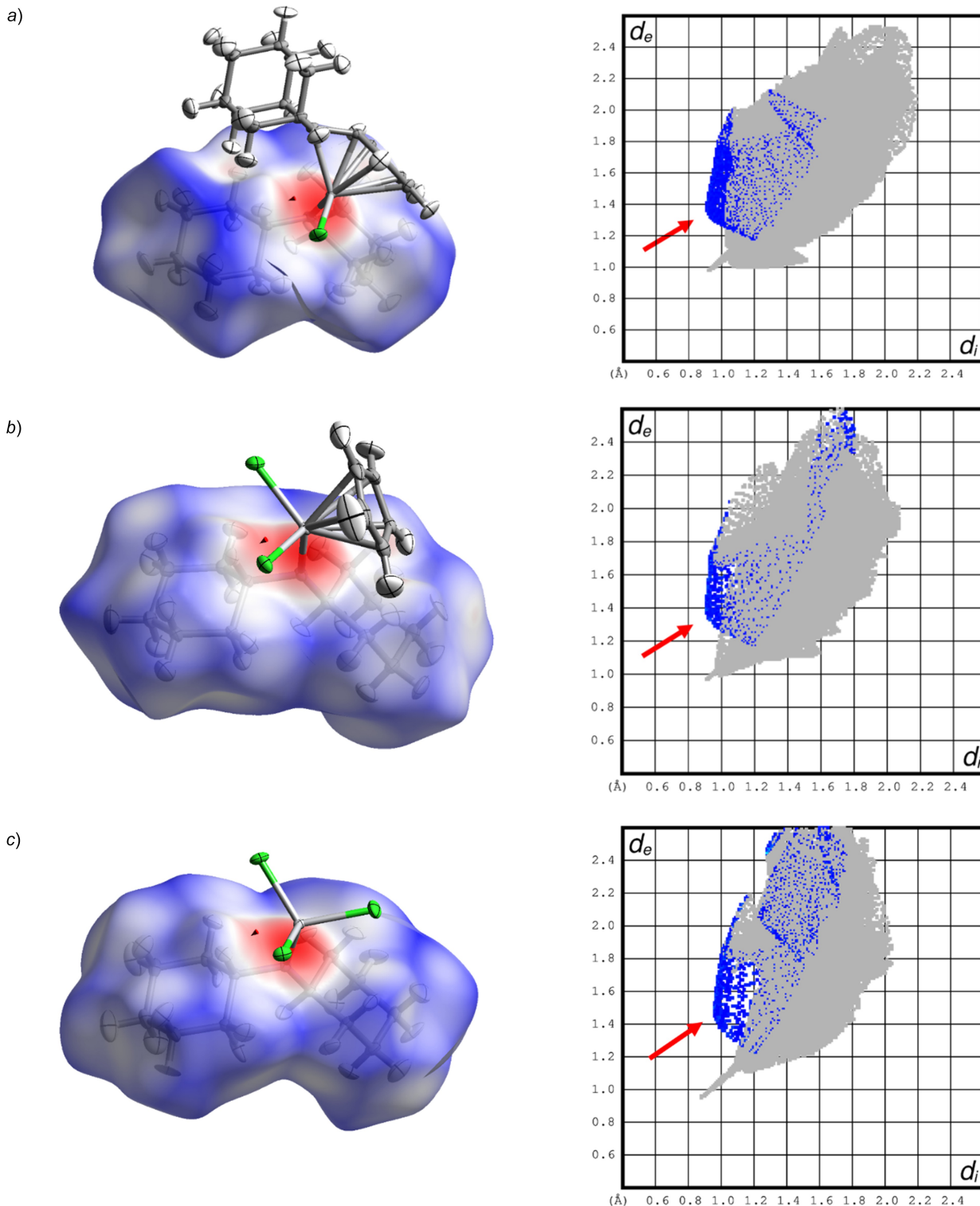
Figure 4. Hirshfeld surfaces and fingerprint plots of the amide ligand for (*a*) **1**, (*b*) **2**, (*c*) **3**. *Hirshfeld* surfaces color coded with the property d$_{norm}$ in a range from −0.91/−0.93/−0.96 (red) to zero (white) to 1.53/1.39/1.30 (**1/2/3**). The red arrows highlight the regions of the C−H···Ti close contacts.
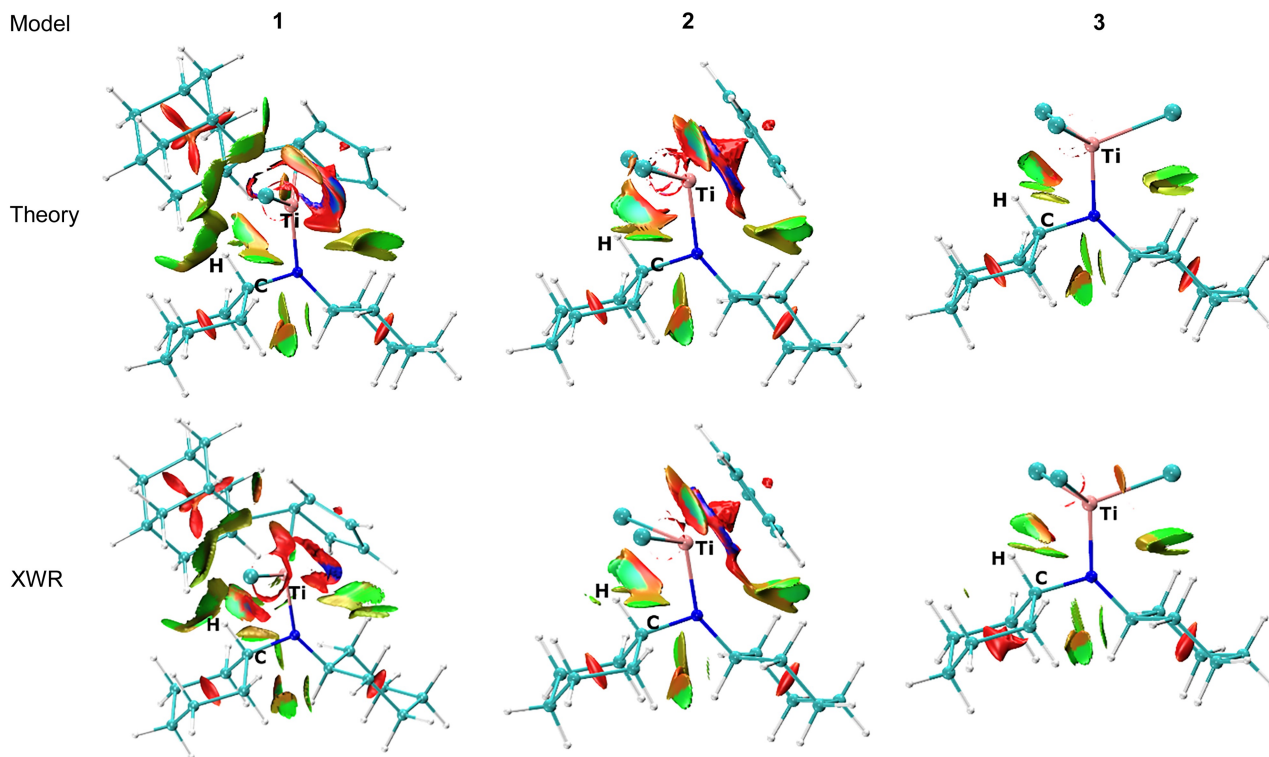
Figure 5. Iso-surface representations of the non-covalent interaction (NCI) index. Sign(λ_2)·ϱ is mapped onto the reduced density gradient iso-surface s(r) = 0.5. Steric (repulsive) interactions (red), attractive electrostatic interactions (blue), weak van-der-Waals interactions (green/brown). Atom types: rose = Ti; blue = N; light blue = C and Cl; white = H.

London dispersion (additional covalent bonding/charge transfer is not visible in the NCI representation) and repulsion through steric crowding (*Pauli* repulsion).
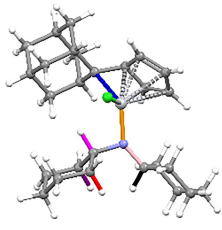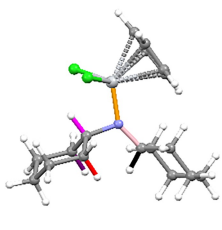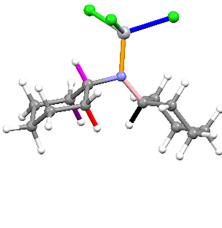
Importantly, according to the NCI index, the C–H···Ti interaction is not the dominant factor in the stabilization of the given conformation of the molecules. London dispersion between the ligands determines the conformation: between the two hexyl groups (in the pictures underneath the N-atoms), between C–H groups and Cl-atoms (in **3**, especially on the side of the molecule without the agostic interaction), between the cyclohexyl and the cyclopentadienyl ligands in **1** and **2**, and, in **1**, very strongly between the agostic C–H bond in question and the adamantyl cage. This means that the design of the ligand system is crucial to bring a C–H bond into proximity of the Ti-atom and this, in turn, activates the C–H bond.

To shed further light on the intramolecular donor-acceptor interactions, we performed NBO analysis. NBO analysis gives insight into charge transfer between atoms through orbital overlap and is hence complementary to the NCI index that depicts electro-

static and *van-der-Waals* interactions only. As *Table 4* shows, here the dominating donor-acceptor interaction is the agostic interaction of type σ(C–H)→LV/RY(Ti) (LV = lone valence orbital, RY = Rydberg orbital). It is a hyperconjugative interaction in which charge is transferred from the C–H σ-bond to an unoccupied orbital located at the Ti-atom. This is in contrast to a hydrogen bonding interaction where lone pair density of a hetero atom is transferred to the X–H antibonding σ-orbital (LP(Y)→σ*(X–H)). Whereas all the other interactions do not exceed 20 kJ/mol, the agostic interactions are between 80 and 180 kJ/mol.

In compound **3**, however, the main mechanism of the agostic interaction is not of σ(C–H)→LV/RY(Ti) type but of σ(C–H)→σ*(Ti–Cl) type, as this is the only compound with a Ti–Cl bond oriented in a 90° angle with respect to the C–H bond (180° angle with respect to the H···Ti axis), ideal for orbital overlap. Still, if adding both E(2) energies for σ(C–H)→LV/RY(Ti) and σ(C–H)→σ*(Ti–Cl) up, the agostic interaction in **3** remains the weakest and the one in **1** the strongest by more than 50 kJ/mol difference to **3** and about 20 kJ/mol to **2**. This is in contrast to the order of C–H bond elongation and compliance matrix analysis discussed

Table 4. Second order perturbation theory analysis of the Fock matrix in the NBO basis. The most important interactions in the vicinity of the Ti-atom are listed. The given E(2) energies are a measure of electron delocalization between pairs of NBOs (kJ/mol). LP = lone pair (occupied), LV = lone valency (empty), RY=Rydberg orbital (empty). The bonds belonging to the donor/acceptor NBOs are color coded. The pink C−H bond is the agostic bond in question. Preliminary results for E(2) energies after XCW fitting are shown in the Supporting Information, Table S7.

	Donor	Acceptor	Theory E(2)	SP at HAR geometry E(2)
1	σ(C−H)	LV(Ti)/RY(Ti)	102.1	172.8
	σ(C−H)	σ*(N−C)	17.4	18.2
	σ(C−H)	σ*(C−H)	12.3	13.3
	σ(C−H)	σ*(C−H)	12.1	13.5
	σ(C−H)	σ*(C−H)	15.1	16.2
	σ(C−H)	σ*(C−H)	14.3	16.4
	σ(C−H)	σ*(C−H)	2.9	3.1
	LP(N)	σ*(C−H)	9.3	13.0
	σ(Ti−C)	σ*(C−H)	4.4	4.0
	σ(N−C)	σ*(C−H)	5.6	6.7
2	σ(C−H)	LV(Ti)/RY(Ti)	87.2	158.1
	σ(C−H)	σ*(N−C)	15.0	16.5
	σ(C−H)	σ*(C−H)	13.2	14.1
	σ(C−H)	σ*(C−H)	13.4	14.0
	σ(C−H)	σ*(C−H)	13.3	14.3
	σ(C−H)	σ*(C−H)	13.3	14.5
	σ(C−H)	σ*(C−H)	4.0	3.4
	LP(N)	σ*(C−H)	N/A	8.5
	σ(N−C)	σ*(C−H)	6.7	6.2
3	σ(C−H)	LV(Ti)/RY(Ti)	12.4	23.9
	σ(C−H)	σ*(Ti−Cl)	47.4	79.6
	σ(C−H)	σ*(Ti−N)	N/A	2.2
	σ(C−H)	σ*(N−C)	17.1	18.9
	σ(C−H)	σ*(C−H)	12.8	14.6
	σ(C−H)	σ*(C−H)	12.8	15.5
	σ(C−H)	σ*(C−H)	14.0	15.4
	σ(C−H)	σ*(C−H)	13.9	15.2
	σ(C−H)	σ*(C−H)	2.2	N/A
	σ(Ti−N)	σ*(C−H)	3.8	4.3
	σ(N−C)	σ*(C−H)	5.9	6.2

above, which was **1** > **3** > **2**. This shows that the aspect of orbital overlap and charge transfer sampled with NBO is complementary to the methods discussed so far.

Another striking feature in the E(2) delocalization energies in *Table 4* is the significant impact of the geometry on the values for the agostic interactions. The agostic interactions are nearly twice as strong at the fixed experimental geometries compared to the optimized geometries; and this is not the case for any other interaction shown in the table. This means that the C−H bond elongation is crucial for the strength of the agostic bonds, which highlights the failure of DFT to reproduce the experimental C−H bond distances (see *Table 1*). However, this can only be one of the factors for the significantly higher E(2) energies, but it cannot be the only one as the SP and optimized results agree in the order of the E(2) energies **1** > **2** > **3**, whereas in terms of C−H bond elongation it is **1** > **3** > **2**. Hence, an adjustment of the overall conformations must be another reason (see *Figure S6* in the *Supporting Information*).

Related to this point, there are two more noteworthy observations with respect to *Table 4*. The first is that there are many additional intramolecular interactions donating electron density from the adjacent C−H, N−C, Ti−C, and Ti−N bonds as well as the nitrogen lone pair into the antibonding orbital of the agostic C−H bond (pink color). This weakens and elongates this bond in addition to the agostic interaction. The second observation is that there are numerous inter-ligand interactions between 10 and 20 kJ/mol each that add up to a very significant stabilization of the respective conformations of the

molecules. This is the complementary viewpoint of the discussion related to the NCI index plots in Figure 5. Only some of those additional interactions that involve the agostic C–H bond in question are shown in *Table 4*, but there are so many of similar kind with different C–H bonds (σ(C–H)$\rightarrow\sigma$*(C–H/Ti–N/Ti–C/N–C)) that they cannot be listed neither here nor in the *Supporting Information*.

As QTAIM is often used to discuss agostic interactions, we produced the molecular graphs and topological electron-density properties for **1** to **3** as well. They are very similar between pure theory and XWR, so only the XWR ones are shown and discussed here (*Figure 6*). The main observation is that there are no bond paths between the Ti-atom and any of the two atoms of the C–H bond. Since we have demonstrated above that the agostic interactions are certainly reality, it shows that the occurrence of QTAIM bond paths is neither a necessary nor a useful criterion for the existence of agostic interactions. However, those additional weak intramolecular ligand-ligand interactions discussed before are represented through bond paths (dotted lines), and are especially prom-
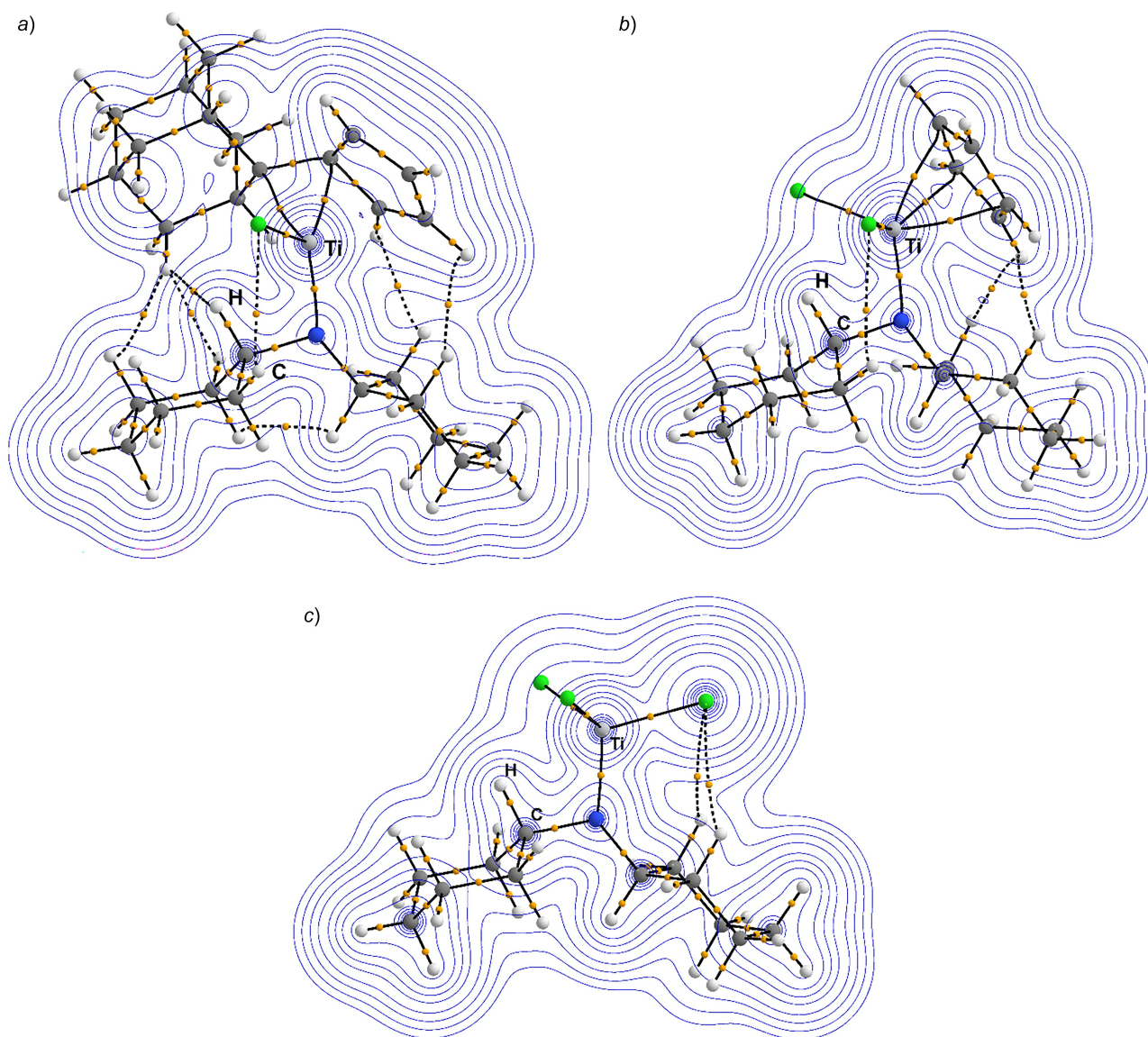

Figure 6. QTAIM molecular graphs with bond paths and bond critical points (BCPs) on a two-dimensional electron-density contour map. Only from XWR, purely theoretical ones are given in the *Supporting Information*, *Figure S2*. Orange = BCP. Electron density contour line value = 0.1 a.u., minimum contour of 0.0001 a.u.

inent in **1**, in agreement with both NCI and NBO analysis.

For **1** and **3**, the hydrogen atom in the agostic interaction has a slightly negative QTAIM atomic charge, whereas the respective hydrogen atom not involved in any intramolecular interaction (see insert of *Table 2* for its identification) has a slightly positive charge (for **1**, -0.04 e *vs.* 0.00 e; for **3**, -0.01 e *vs.* $+0.01$ e), whereas this trend does not hold for **2**. Likewise, in **1** and **3** the C–H bond involved in the agostic interaction has a slightly lower electron density value at the bond critical point than the respective one not involved in agreement with bond weakening (for **1**, 1.805 e Å^{-3} *vs.* 1.918 e Å^{-3}; for **3**, 1.809 e Å^{-3} *vs.* 1.911 e Å^{-3}), whereas this again does not hold for **2**. This trend agrees with the trend that the C–H bond elongation in **2** is significantly less pronounced than in **1** and **3** (*Table 1*).

As discussed by *Scherer et al.* previously based on the Laplacian of the electron density, the field of ligands induces charge concentrations in the outer core or valence shell of the metal ion (LICCs = ligand-induced charge concentrations), roughly in projection of the bond direction at the rear side of the atom.[25]

The agostic C–H bond then points towards a charge depletion zone between these LICCs to fill a local vacancy in the coordination shell.[24] Some of us have shown previously that this can also be represented by the electron localizability indicator ELI (termed LICLs = ligand-induced charge localizations),[63] because ELI and Laplacian of electron density nearly always show isomorphous mapping (except in highly correlated systems).[64]

Here, we show three-dimensional representations of localization domains of ELI in *Figure 7*. Since hydrogen has no core electrons, the C–H bond is formed as a protonated monosynaptic valence basin. It is populated with 2.03 (**1**), 1.99 (**2**), 2.00 (**3**) electrons (XWR). The non-agostic C–H bond (for its definition and location, see insert in *Table 2*) has virtually the same electron population (2.02 (**1**), 1.96 (**2**), 1.99 e (**3**)). However, despite the same population, the volumes of the respective basins are much smaller in the case of the agostic C–H bond, which shows the impact of the bonded interaction to the Ti-atom and hence the C–H activation (53.8 *vs.* 57.4 a$_0^3$ (**1**); 47.0 *vs.* 54.2 a$_0^3$ (**2**); 55.5 *vs.* 54.2 a$_0^3$ (**3**)). Here, **3** is an exception, as will
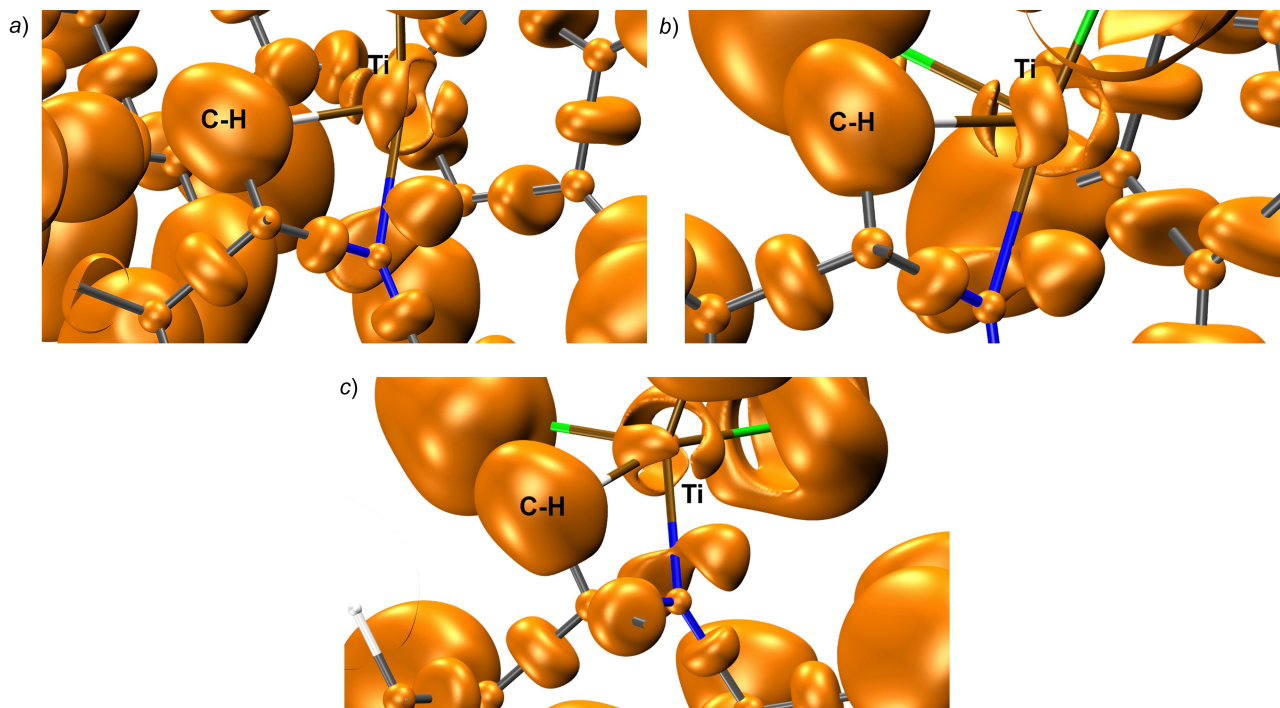
Figure 7. ELI–D localization domain representations at an ELI isosurface value of 1.5. Only from XWR, purely theoretical ones are given in the *Supporting Information* (*Figure S4*). The agostic interaction is represented by a stick as for the other bonds to visualize the straight bond axis between H- and Ti-atoms. All irreducible localization domains presented here represent an electron-pair basin (such as bonds, lone pairs and the shell structure of the atomic cores). For more details on the chemical interpretation of the features, we refer to a didactic review paper about the electron localization function ELF.[65]

also be discussed in the following paragraph. More details about ELI–D are collected in *Table S6*.

The formally d^0 Ti ion has a structured outer core region of between 3.5 and 4.5 electrons not provided for covalent bonding with the C/N/Cl partners (*Figure 7*, *Table S6*). One could argue that these are the valence electrons of Ti that give rise to non-VSEPR structures.[66] Anyway, in compounds **1** and **2**, the direct bond axis between H- and Ti-atoms is directed towards a local charge depletion zone at the Ti-atom as discussed as one of the criteria for the occurrence of agostic interactions in the Introduction. However, for **3** this is not the case as there is a LiCl generated by one of the Cl ligands in the H⋯Ti bond axis. This difference between charge depletion and accumulation in the H⋯Ti bond axis of **1**, **2** and **3** is likewise visible in the distribution of the Laplacian of the electron density (*Figure S3* in the *Supporting Information*). This is another sign that the agostic bonding mechanism in **3** is different because of the occurrence of an additional Cl ligand in 90° angle to the C–H bond and 180° angle to the H⋯Ti axis, as discovered in the context of NBO analysis.

Conclusions and Outlook

Barnett et al. stated still in 2019 that 'X-ray analysis is not sufficient enough to conclude without any doubt the existence of an agostic bond due to the well-known problem of determining the exact position of a H next to the much heavier TM'.[67] We disagree with this statement because the authors imply that X-ray analysis means application of the inadequate IAM refinement. In this work, we have shown that X-ray analysis with a more adequate model such as HAR indeed allows to determine the positions of the hydrogen atoms in a C–H bond accurately and precisely enough to detect an elongation of the C–H bond and a shortening of the C–H⋯Ti angle towards 90°. This means that we can 'conclude without any doubt the existence of an agostic bond' in the vicinity of the light transition metal Ti. Some specialized work on agostic interactions with heavier transition metals using quantum crystallography has been published very recently,[48,49] but this could now be approached more systematically and more frequently.

This article gives reliable experimental reference values for geometrical parameters in C–H⋯Ti interactions for the first time, since no neutron diffraction data are available for this textbook agostic system in the literature. We also show in this article that the

geometry optimization featuring the standard DFT functional B3LYP fails in reproducing both the HAR-derived C–H bond elongation and the NBO delocalization energies. In the HAR geometries, the E(2) energies are approximately twice as high as in the optimized geometries. As until now no reference values were available, this failure of theory could not have been discovered or discussed before. We will address it more systematically in future studies by resorting to fully periodic calculations and/or highly correlated post-HF methods in comparison to results from X-ray wavefunction refinement.

However, despite the fact that the elongation of the C–H bonds is reliable and consistent, it is not statistically significant, *i.e.*, not outside three times the standard uncertainties obtained from the refinement procedure. Therefore, further electronic and spectroscopic criteria must be discussed for a classification of the bonds as being agostic and for an estimation of the C–H⋯Ti bond strengths. Whereas all descriptors that are more or less directly related to the C–H bond distance (such as the compliance matrix analysis or QTAIM) show the order of agostic bond strength as **1** > **3** > **2**, the NBO and ELI analyses show an aspect of the agostic interaction complementary to the geometrical analysis; they reveal a different charge-transfer mechanism that goes through a Ti–Cl bond in a 180° angle relative to the H⋯Ti axis rather than unoccupied orbitals at the Ti-atom. As a consequence, the order according to these methods is **1** > **2** > **3**. In general, geometric criteria alone can in some cases identify the existence of an agostic interaction but cannot sufficiently characterize it. In this context, it is noteworthy that **1** and **2** rather exist in a *pseudo*-octahedral coordination environment, whereas **3** rather in a *pseudo*-tetrahedral one. This has, in turn, been shown previously to have some effect on the agostic interaction strength as different orbitals are more vacant or more populated.[68]

All used bonding descriptors that are designed to identify and characterize weak intramolecular interactions (NCI, NBO, QTAIM) find that beyond the agostic interaction a large number of further ligand-ligand interactions is crucial for the stabilization of the conformation, both in terms of London dispersion and charge transfer. It seems plausible that the introduction of bulky alkylic ligands such as the adamantly group in **1** cause the C–H⋯Ti interaction to be stronger and thus present a possible design motif for other strongly agostic systems.

Experimental and Computational Section

Synthesis and Crystallization

All reactions were performed in an inert atmosphere of argon or nitrogen with the rigorous exclusion of oxygen and moisture by using standard glovebox and *Schlenk* techniques. Nonhalogenated solvents were dried with sodium/benzophenone and freshly distilled prior to use. Dicyclohexylamine was distilled and stored under a nitrogen atmosphere. ^{1}H- and ^{13}C-NMR spectra were recorded with a *Bruker AVANCE III 500* spectrometer (^{1}H 500.1 MHz, ^{13}C 125.8 MHz) or a *Bruker AVANCE 300* spectrometer (^{1}H 300.1 MHz). Further details for compounds **1** and **3** have been described previously.[16] Compound **2** has been obtained by reaction of $CpTiCl_3$ (1 g, 4.6 mmol) in 50 mL THF as solvent with 0.85 g Cy_2NLi (4.6 mmol) at 60 °C. After 2 h, the solvent was removed, and the residue extracted by 70 ml of hexane. After filtration and cooling to 0 °C, **2** was obtained in the form of dark red needles (1.26 g (76%). M.p. 154 °C (dec.)). ^{1}H-NMR (300 MHz, 300 K, C_6D_6): 0.88–1.71 (m, 20H, CH_2), 4.57 (br. s, 2H, NCH), 6.34 (s, 5H, C_5H_5). ^{13}C-NMR (75.5 MHz, 300 K, C_6D_6): 25.8 (Cγ, Cy), 27.0 (Cβ, Cy), 33.6 (Cα, Cy), 63.8 (N$\underline{C}$H, Cy), 117.2 ($\underline{C}_5H_5$). EI-MS (70 eV): 363 (35, M^+), 327 (100, $[M-Cl]^+$), 297 (85, $[M-Cp]^+$), 180 (95, $[CyN]^+$), 138 (85), 98 (38), 83 (80, $[Cy]^+$), 65 (8, $[Cp]^+$).

Crystallography

Previously reported X-ray diffraction data for **1** were used.[16] New data sets were collected for both **2** and **3** using Mo–Kα radiation on a *Bruker APEX2* diffractometer equipped with a CCD detector at a temperature of 100 K up to a resolution of d = 0.62 Å. Numerical absorption corrections followed by empirical absorption corrections were applied using SADABS.[69] Cell parameters were refined using the Bruker SAINT program.[70] Structure solution for the new structures was performed using SHELXT[71] and initially all refinements were performed using the SHELXL[72] software in the independent atom model (IAM). The structure refinement of compound **3** includes the refinement of a 2-component twin with a 2-fold rotation twin law. All pertinent details regarding the data collection can be found in *Table S2* in the *Supporting Information*.

The models obtained from the refinement using SHELXL were further subjected to an IAM in the software Tonto[73] against structure factor magnitudes F, releasing all coordinates and isotropic displacement parameters for the hydrogen atoms and applying a $1/\sigma^2(F)$ weighting scheme without fudge parameters. The reflection file of compound **3** was de-twinned using a self-written script before it was used in Tonto. Final IAM geometries for all compounds were used as input for HAR using the interface lamaGOET[74] with Gaussian09[75]/Tonto as engines for the quantum chemical calculations/refinements. The B3LYP/def2-TZVP level of theory was selected in Gaussian09. Crystal environmental effects were simulated by the inclusion of a self-consistent field of cluster charges of 8 Å around the central molecule. Hydrogen atoms were treated anisotropically. Analysis of the final structure according to Hirshfeld surface analysis[60] was carried out in the software CrystalExplorer.[76]

XWR was performed as a sequence of HAR and XCW fitting, here using the software lamaGOET as a GUI to Tonto. The XCW fittings were carried out using the HF/def2-TZVP level of theory, without a surrounding cluster of point charges and dipoles. The philosophy for this change in the quantum-mechanical method is that the effects of electron correlation, polarization and relativistics are included in the *Hartree-Fock* wavefunction during the XCW fitting process.[77] The refinement details given in *Table 5* show that there is a massive drop in the statistical *R*-values and goodness-of-fit (GooF) parameters from IAM to HAR upon inclusion of non-spherical bonding and non-bonding effects in the model. The same statistical parameters improve significantly again from HAR to XWR upon additional inclusion of mainly the physical effects electron correlation and polarization. This also reduces the maximum residual electron density significantly that was not affected as much from IAM to HAR. The critical meaning of the parameter λ that controls the XCW fitting is discussed in ref.[53] and ref.[78]. Here, fitting was terminated at maximum λ values of 0.34/0.70/0.90, referring to the last point before convergence of the constrained self-consistent field (SCF) calculations ceased. The final crystallographic information files (CIFs) after XWR can be downloaded from the Cambridge Structural Database at https://www.ccdc.cam.ac.uk/structures/under entries CCDC-2238208-2238209/2238211-2238212/2238213-2238214 (HAR-XWR **1/2/3**).

Computational Part

Theoretical geometry optimizations for all three compounds were performed in Gaussian09[75] using the final HAR geometries as initial guesses. Optimizations were performed for the isolated molecule (gas-phase

Table 5. Refinement statistics.

	1	**2**	**3**
Tonto IAM			
Number of parameters	431	298	242
Number of unique obs.[a]	8668	5394	5862
R factor (obs)	0.0278	0.0296	0.0323
w*R* factor (obs)	0.0284	0.0231	0.0265
GooF^2	16.34	7.15	8.05
GooF	4.04	2.67	2.84
Residual density max [e/Å^3]	0.442	0.475	0.624
Residual density min [e/Å^3]	−0.377	−0.406	−0.448
Residual density mean [e/Å^3]	0.047	0.043	0.083
HAR			
Number of parameters	631	433	352
Number of unique obs.	8668	5394	5862
R factor (obs)	0.0155	0.0225	0.0276
w*R* factor (obs)	0.0118	0.0152	0.0195
GooF^2	2.91	3.19	4.43
GooF	1.71	1.79	2.10
Residual density max [e/Å^3]	0.315	0.458	0.636
Residual density min [e/Å^3]	−0.224	−0.375	−0.384
Residual density mean [e/Å^3]	0.027	0.034	0.076
XWR			
R factor (obs)	0.0130	0.0189	0.0239
w*R* factor (obs)	0.0086	0.0109	0.0144
λ_{max}	0.34	0.70	0.90
GooF^2	1.53	1.63	2.41
GooF	1.24	1.28	1.55
Residual density max [e/Å^3]	0.205	0.424	0.424
Residual density min [e/Å^3]	−0.259	−0.322	−0.386
Residual density mean [e/Å^3]	0.024	0.034	0.067

[a] obs = cutoff criterion of F > 3σ(F).

model labeled **G** below). In addition, optimizations were set up using the routines inside lamaGOET where the interfacing with Tonto allows the simulated surrounding cluster of point Hirshfeld charges to be used during the optimizations inside the software Gaussian09. The automated procedure[74] performs several optimizations updating the self-consistent field (SCF) of cluster charges until there are no deviations on geometry or final energy values anymore. The procedure can use *Hirshfeld* charges described as monopoles (**M**) or expanded up to a dipole (**D**) level. In addition, empirical dispersion correction according to the GD3BJ method can be selected. In this study, the following series of theory levels was used for the optimization of compounds **1** to **3**, with the model abbreviation given in bold font in square brackets:

- B3LYP/6-311+G(2df,p) [**G**]
- B3LYP/6-311+G(2df,p)+SCF of *Hirshfeld* charges (monopoles only) of 8 Å radius [**M**]
- B3LYP/6-311+G(2df,p)+SCF of *Hirshfeld* charges (monopoles and dipoles) of 8 Å radius [**M+D**]

- Any level above+GDB3J empirical dispersion correction (**G/M/M+D+Emp**)

Compliance matrix analysis was carried out with the Compliance software[79] based on the Hessian matrix obtained in Gaussian09 from frequency analysis. NBO analysis was carried out with the software NBO7.[80] For electron-density plots and QTAIM analysis, the software AIMAll[81] was used. The NCI index was calculated with Multiwfn[82] and visualized with VMD.[83] The ELI was calculated and integrated with DGrid[84,85] and also visualized with VMD.

Properties from the Fitted Wavefunction

The same software programs as listed in the previous paragraph were used for the calculation of properties from the XCW fitted wavefunction. However, the software Tonto does not perform frequency analysis, hence, compliance matrix analysis was not possible after XWR. Within an NBO analysis, the *Fock* matrix is necessary for second order perturbation calculations on the *Fock* matrix in the NBO basis. Although the *Fock* matrix output by Tonto contains the entire matrix divided into blocks according to the number of orbitals in the system, this format is not readable for NBO7. Therefore, we have written a bash script that will rearrange the output of the entire *Fock* matrix into the required half diagonal matrix format for a .47 file that can be read directly by the NBO (6.0 or 7.0) program. The results were consistent between XWR wavefunction and pure theory except for electron donation into Rydberg orbitals where the XWR-derived numbers seem unreasonably high. For this reason, we consider the results as preliminary and only discuss them in the *Supporting Information*, *Table S7*. In addition to the results from the geometry optimizations and the XWR, single-point theoretical calculations of **1** to **3** at the B3LYP/def2-TZVP and HF/def2-TZVP level of theory were performed upon fixing the coordinates after HAR.

Supplementary Material

Supporting information for this article is available on the WWW under https://doi.org/10.1002/hlca.202300012. It contains a pdf document with more details about crystallography and bonding descriptors. The crystallographic information files (CIFs) that contain the final XWR structures of **1** to **3** have been deposited with the Cambridge Structural Database

HELVETICA
chimica acta

under deposition numbers CCDC-2238208-09 and 2238211–14.

Acknowledgements

Data Availability Statement

Data are available at the Cambridge Crystallographic Data Centre and as supporting information of this article.

Author Contribution Statement

L. A. Malaspina carried out the quantum crystallographic and quantum chemical refinements and calculations, interpreted the results and prepared graphics and tables. *N. Frerichs* and *C. Adler* equally contributed to the preparation of compounds **1**–**3**. *M. Schmidtmann* performed the single-crystal X-ray diffraction experiments and carried out the initial IAM refinements. *R. Beckhaus* supervised the synthetic part of the study and contributed to the text. *S. Grabowsky* supervised the quantum crystallographic and bonding analysis part of the study and wrote the manuscript.

References

[1] J. Halpern, 'Activation of carbon-hydrogen bonds by metal complexes: Mechanistic, kinetic and thermodynamic considerations', *Inorg. Chim. Acta* **1985**, *100*, 41–48.

[2] R. H. Crabtree, 'Transition Metal Complexation of σ Bonds', *Angew. Chem. Int. Ed.* **1993**, *32*, 789–805.

[3] G. J. Kubas, 'Metal Dihydrogen and σ-Bond Complexes', 'Modern Inorganic Chemistry' series, Kluwer Academic/Plenum Publishers, New York, 2001.

[4] K. Mashima, A. Nakamura, 'Agostic interaction in early transition metal alkyls and their role in catalytic activity for olefin polymerizations', *J. Organomet. Chem.* **1992**, *428*, 49–58.

[5] M. Brookhart, M. L. H. Green, 'Carbon-hydrogen-transition metal bonds', *J. Organomet. Chem.* **1983**, *250*, 395–408.

[6] Z. Dawoodi, M. L. H. Green, V. S. B. Mtetwa, K. Prout, A. J. Schultz, J. M. Williams, T. F. Koetzle, 'Evidence for carbon–hydrogen–titanium interactions: synthesis and crystal structures of the agostic alkyls [TiCl₃(Me₂PCH₂CH₂PMe₂)R] (R=Et or Me)', *J. Chem. Soc., Dalton. Trans.* **1986**, 1629–1637.

[7] Z. Dawoodi, M. L. H. Green, V. S. B. Mtetwa, K. Prout, 'Evidence for a direct bonding interaction between titanium and a β-C–H moiety in a titanium–ethyl compound; X-ray crystal structure of [Ti-(Me₂PCH₂CH₂PMe₂)EtCl₃]', *J. Chem. Soc., Chem. Commun.* **1982**, 802–803.

[8] X. Lin, W. Wu, Y. Mo, 'A theoretical perspective of the agostic effect in early transition metal compounds', *Coord. Chem. Rev.* **2020**, *419*, 213401.

[9] A. Haaland, W. Scherer, K. Ruud, G. S. McGrady, A. J. Downs, O. Swang, 'On the Nature and Incidence of β-Agostic Interactions in Ethyl Derivatives of Early Transition Metals: Ethyltitanium Trichloride and Related Compounds', *J. Am. Chem. Soc.* **1998**, *120*, 3762–3772.

[10] W. Scherer, D, J. Wolstenholme, V. Herz, G. Eickerling, A. Brück, P. Benndorf, P. W. Roesky, 'On the Nature of Agostic Interactions in Transition-Metal Amido Complexes', *Angew. Chem. Int. Ed.* **2010**, *49*, 2242–2246.

[11] X. Lin, W. Wu, Y. Mo, 'Agostic Interactions in Early Transition-Metal Complexes: Roles of Hyperconjugation, Dispersion, and Steric Effect', *Chem. Eur. J.* **2019**, *25*, 6591–6599.

[12] W. Scherer, W. Hieringer, M. Spiegler, P. Sirsch, G. S. McGrady, A. J. Downs, A. Haaland, B. Pedersen, 'Characterisation of agostic interactions by a topological analysis of experimental and theoretical charge densities in [EtTiCl₃(dmpe)] [dmpe=1,2-bis(dimethylphosphino)ethane]', *Chem. Commun.* **1998**, 2471–2472.

[13] S. Scheins, M. Messerschmidt, M. Gembicky, M. Pitak, A. Volkov, P. Coppens, B. G. Harvey, G. C. Turpin, A. M. Arif, R. D. Ernst, 'Charge Density Analysis of the (C–C)→Ti Agostic Interactions in a Titanacyclobutane Complex', *J. Am. Chem. Soc.* **2009**, *131*, 6154–6160.

[14] E. Chong, P. Garcia, L. L. Schafer, 'Hydroaminoalkylation: Early-Transition-Metal-Catalyzed α-Alkylation of Amines', *Synthesis* **2014**, *46*, 2884–2896.

[15] M. Manßen, N. Lauterbach, J. Dörfler, M. Schmidtmann, W. Saak, S. Doye, R. Beckhaus, 'Efficient Access to Titanaaziridines by C–H Activation of *N*-Methylanilines at Ambient Temperature', *Angew. Chem. Int. Ed.* **2015**, *54*, 4383–4387.

[16] C. Adler, A. Bekurdts, D. Haase, W. Saak, M. Schmidtmann, R. Beckhaus, 'Bulky Titanium Amides: C–H Bond Activation under Mild Conditions', *Eur. J. Inorg. Chem.* **2014**, 1289–1302.

[17] W. Scherer, V. Herz, C. Hauf, 'On the Nature of β-Agostic Interactions: A Comparison Between the Molecular Orbital and Charge Density Picture', in 'Electron Density and Chemical Bonding I. Structure and Bonding', Vol. 146, Ed. D. Stalke, Springer, Berlin, Heidelberg, 2012, pp. 159–207.

[18] M. Brookhart, M. L. H. Green, G. Parkin, 'Agostic interactions in transition metal compounds', *Proc. Natl. Acad. Sci. USA* **2007**, *104*, 6908–6914.

[19] I. Corral, O. Mó, M. Yáñez, 'Agostic vs π-Interactions in Complexes of Ethynylsilanes and Ethynylgermanes with Cu⁺ in the Gas Phase', *J. Phys. Chem. A* **2003**, *107*, 1370–1376.

[20] G. von Frantzius, R. Streubel, K. Brandhorst, J. Grunenberg, 'How Strong Is an Agostic Bond? Direct Assessment of

Agostic Interactions Using the Generalized Compliance Matrix', *Organometallics* **2006**, *25*, 118–121.

[21] J. E. Barquera-Lozada, A. Obenhuber, C. Hauf, W. Scherer, 'On the Chemical Shifts of Agostic Protons', *J. Phys. Chem. A* **2013**, *117*, 4304–4315.

[22] R. F. W. Bader, 'Atoms in molecules', *Acc. Chem. Res.* **1985**, *18*, 9–15.

[23] M. Jabłoński, 'QTAIM-Based Comparison of Agostic Bonds and Intramolecular Charge-Inverted Hydrogen Bonds', *J. Phys. Chem. A* **2015**, *119*, 4993–5008.

[24] W. Scherer, G. S. McGrady, 'Agostic Interactions in d^0 Metal Alkyl Complexes', *Angew. Chem. Int. Ed.* **2004**, *43*, 1782–1806.

[25] W. Scherer, P. Sirsch, D. Shorokhov, M. Tafipolsky, G. S. McGrady, E. Gullo, 'Valence Charge Concentrations, Electron Delocalization and β-Agostic Bonding in d^0 Metal Alkyl Complexes', *Chem. Eur. J.* **2003**, *9*, 6057–6070.

[26] E. D. Glendening, C. R. Landis, F. Weinhold, 'Natural bond orbital methods', *WIREs Comput. Mol. Sci.* **2012**, *2*, 1–42.

[27] A. Savin, R. Nesper, S. Wengert, T. F. Fässler, 'ELF: The Electron Localization Function', *Angew. Chem. Int. Ed.* **1997**, *36*, 1808–1832.

[28] M. Kohout, 'A measure of electron localizability', *Int. J. Quantum Chem.* **2004**, *97*, 651–658.

[29] E. R. Johnson, S. Keinan, P. Mori-Sánchez, J. Contreras-García, A. J. Cohen, W. Yang, 'Revealing Noncovalent Interactions', *J. Am. Chem. Soc.* **2010**, *132*, 6498–6506.

[30] M. Lein, 'Characterization of agostic interactions in theory and computation', *Coord. Chem. Rev.* **2009**, *253*, 625–634.

[31] T. S. Thakur, G. R. Desiraju, 'Theoretical investigation of C—H···M interactions in organometallic complexes: A natural bond orbital (NBO) study', *J. Mol. Struct. THEOCHEM* **2007**, *810*, 143–154.

[32] T. Debnath, T. Ash, T. Banu, A. K. Das, 'Investigation of agostic interaction through NBO analysis and its impact on β-hydride elimination and dehydrogenation: a DFT approach', *Theor. Chem. Acc.* **2016**, *135*, 175.

[33] D. C. Najera, M. N. Peñas-Defrutos, M. García-Melchor, A. R. Fout, 'γ-Agostic interactions in (^{Mes}CCC)Fe—Mes(L) complexes', *Chem. Commun.* **2022**, *58*, 9626–9629.

[34] W. Scherer, V. Herz, A. Brück, C. Hauf, F. Reiner, S. Altmannshofer, D. Leusser, D. Stalke, 'The Nature of β-Agostic Bonding in Late-Transition-Metal Alkyl Complexes', *Angew. Chem. Int. Ed.* **2011**, *50*, 2845–2849.

[35] Cambridge Structural Database, accessed January 19th, 2023. C. R. Groom, I. J. Bruno, M. P. Lightfoot, S. C. Ward, 'The Cambridge structural database', *Acta Crystallogr. Sect. B* **2016**, *72*, 171–179.

[36] F. H. Allen, I. J. Bruno, 'Bond lengths in organic and metal-organic compounds revisited: X—H bond lengths from neutron diffraction data', *Acta Crystallogr., Sect. B* **2010**, *66*, 380–386.

[37] W. W. Lukens, P. T. Matsunaga, R. A. Andersen, 'Synthesis and Structure of Cp*$_2$TiH, Cp*$_2$TiH$_2$Li(tmed), and [Cp*$_2$TiOLi(THF)]$_2$', *Organometallics* **1998**, *17*, 5240–5247.

[38] S. R. Frerichs, B. K. Stein, J. E. Ellis, 'Highly Reduced Organometallics. 19. Synthesis of Carbonyl Anions of Titanium(0) from Titanocene Dicarbonyl. The First Structural Characterization of a Carbonyl Hydride of Titanium, (C$_5$H$_5$)Ti-(CO)$_2$(Me$_2$PCH$_2$CH$_2$PMe$_2$)H', *J. Am. Chem. Soc.* **1987**, *109*, 5558–5560.

[39] N. N. Ho, R. Bau, C. Plecnik, S. G. Shore, X. Wang, A. J. Schultz, 'A neutron diffraction study of Cp$_2$Ti{(μ-H)$_2$BC$_8$H$_{14}$}', *J. Organomet. Chem.* **2002**, *654*, 216–220.

[40] G. M. Sheldrick, 'A short history of *SHELX*', *Acta Crystallogr. Sect. A* **2008**, *64*, 112–122.

[41] F. Akagi, T. Matsuo, H. Kawaguchi, 'Titanium and Zirconium Complexes of Reorganized Tripodal Triaryloxide Ligands', *J. Am. Chem. Soc.* **2005**, *127*, 11936–11937.

[42] M. Woińska, S. Grabowsky, P. M. Dominiak, K. Woźniak, D. Jayatilaka, 'Hydrogen atoms can be located accurately and precisely by x-ray crystallography', *Sci. Adv.* **2016**, *2*, e1600192.

[43] D. Jayatilaka, B. Dittrich, 'X-ray structure refinement using aspherical atomic density functions obtained from quantum-mechanical calculations', *Acta Crystallogr. Sect. A* **2008**, *64*, 383–393.

[44] S. C. Capelli, H.-B. Bürgi, B. Dittrich, S. Grabowsky, D. Jayatilaka, 'Hirshfeld atom refinement', *IUCrJ* **2014**, *1*, 361–379.

[45] L. A. Malaspina, A. Genoni, D. Jayatilaka, M. J. Turner, K. Sugimoto, E. Nishibori, S. Grabowsky, 'The advanced treatment of hydrogen bonding in quantum crystallography', *J. Appl. Crystallogr.* **2021**, *54*, 718–729.

[46] F. Kleemiss, O. V. Dolomanov, M. Bodensteiner, N. Peyerimhoff, L. Midgley, L. J. Bourhis, A. Genoni, L. A. Malaspina, D. Jayatilaka, J. L. Spencer, F. White, B. Grundkötter-Stock, S. Steinhauer, D. Lentz, H. Puschmann, S. Grabowsky, 'Accurate crystal structures and chemical properties from NoSpherA2', *Chem. Sci.* **2021**, *12*, 1675–1692.

[47] M. Woińska, M. L. Chodkiewicz, K. Woźniak, 'Towards accurate and precise positions of hydrogen atoms bonded to heavy metal atoms', *Chem. Commun.* **2021**, *57*, 3652–3655.

[48] S. Holsten, L. A. Malaspina, F. Kleemiss, S. Mebs, E. Hupf, S. Grabowsky, J. Beckmann, 'Different Reactivities of (5-Ph$_2$P-Ace-6-)$_2$MeSiH toward the Rhodium(I) Chlorides [(C$_2$H$_4$)$_2$RhCl]$_2$ and [(CO)$_2$RhCl]$_2$. Hirshfeld Atom Refinement of a Rh–H···Si Interaction', *Organometallics* **2021**, *40*, 2027–2038.

[49] J. Pérez-Pérez, U. Hernández-Balderas, D. Martínez-Otero, M. Moya-Cabrera, V. Jancik, 'Hetero-bimetallic alkali titanosilicates [MOTi{OSi(O^{t}Bu)$_3$}$_3$]$_2$ (M≡Li–Cs) with terminal Ti–O groups', *Dalton Trans.* **2022**, *51*, 6148–6152.

[50] T. S. Koritsanszky, P. Coppens, 'Chemical Applications of X-ray Charge-Density Analysis', *Chem. Rev.* **2001**, *101*, 1583–1628.

[51] D. Jayatilaka, 'Wave Function for Beryllium from X-Ray Diffraction Data', *Phys. Rev. Lett.* **1998**, *80*, 798–801.

[52] D. Jayatilaka, D. J. Grimwood, 'Wavefunctions derived from experiment. I. Motivation and theory', *Acta Crystallogr. Sect. A* **2001**, *57*, 76–86.

[53] M. L. Davidson, S. Grabowsky, D. Jayatilaka, 'X-ray constrained wavefunctions based on Hirshfeld atoms. I. Method and review', *Acta Crystallogr. Sect. B* **2022**, *78*, 312–332.

[54] M. L. Davidson, S. Grabowsky, D. Jayatilaka, 'X-ray constrained wavefunctions based on Hirshfeld atoms. II. Reproducibility of electron densities in crystals of α-oxalic acid dihydrate', *Acta Crystallogr. Sect. B* **2022**, *78*, 397–415.

[55] S. Grabowsky, 'Complementary Bonding Analysis', De Gruyter, Berlin, 2021.

HELVETICA
chimica acta

[56] M. Woińska, D. Jayatilaka, B. Dittrich, R. Flaig, P. Luger, K. Woźniak, P. M. Dominiak, S. Grabowsky, 'Validation of X-ray Wavefunction Refinement', *ChemPhysChem* **2017**, *18*, 3334–3351.

[57] J. D. Dunitz, A. Gavezzotti, 'Molecular Recognition in Organic Crystals: Directed Intermolecular Bonds or Non-localized Bonding?', *Angew. Chem. Int. Ed.* **2005**, *44*, 1766–1787.

[58] J. D. Dunitz, 'Intermolecular atom-atom bonds in crystals?', *IUCrJ* **2015**, *2*, 157–158.

[59] S. S. Batsanov, 'Van der Waals Radii of Elements', *Inorg. Mater.* **2001**, *37*, 871–885.

[60] M. A. Spackman, D. Jayatilaka, 'Hirshfeld surface analysis', *CrystEngComm* **2009**, *11*, 19–32.

[61] M. A. Spackman, J. J. McKinnon, 'Fingerprinting intermolecular interactions in molecular crystals', *CrystEngComm* **2002**, *4*, 378–392.

[62] K. Brandhorst, J. Grunenberg, 'How strong is it? The interpretation of force and compliance constants as bond strength descriptors', *Chem. Soc. Rev.* **2008**, *37*, 1558–1567.

[63] R. Pal, S. Mebs, M. W. Shi, D. Jayatilaka, J. M. Krzeszczakowska, L. A. Malaspina, M. Wiecko, P. Luger, M. Hesse, Y.-S. Chen, J. Beckmann, S. Grabowsky, 'Linear MgCp*$_2$ vs Bent CaCp*$_2$: London Dispersion, Ligand-Induced Charge Localizations, and Pseudo-Pregostic C—H⋯Ca Interactions', *Inorg. Chem.* **2018**, *57*, 4906–4920.

[64] E. Hupf, L. A. Malaspina, S. Holsten, F. Kleemiss, A. J. Edwards, J. R. Price, V. Kozich, K. Heyne, S. Mebs, S. Grabowsky, J. Beckmann, 'Proximity Enforced Agostic Interactions Involving Closed-Shell Coinage Metal Ions', *Inorg. Chem.* **2019**, *58*, 16372–16378.

[65] A. Savin, R. Nesper, S. Wengert, T. F. Fässler, 'ELF: The Electron Localization Function', *Angew. Chem. Int. Ed.* **1997**, *36*, 1808–1832.

[66] M. Kaupp, '"Non-VSEPR" Structures and Bonding in d^0 Systems', *Angew. Chem. Int. Ed.* **2001**, *40*, 3534–3565.

[67] S. Barnett, D. Allan, M. Gutmann, J. Cockcroft, V. Mai, A. Aliev, J. Saßmannshausen, 'Combined high resolution X-ray and DFT Bader analysis to reveal a proposed Ru—H⋯Si interaction in Cp(IPr)Ru(H)$_2$SiH(Ph)Cl', *Inorg. Chim. Acta* **2019**, *488*, 292–298.

[68] O. Eisenstein, Y. Jean, 'Factors Favoring an M⋯H—C Interaction in Metal-Methyl Complexes. An MO Analysis', *J. Am. Chem. Soc.* **1985**, *107*, 1177–1186.

[69] G. M. Sheldrick, 'SADABS-Bruker AXS scaling and absorption correction', Bruker AXS Inc., Madison, WI, USA, 2008.

[70] SAINT, Bruker, 'Data reduction software', Bruker AXS Inc., Madison, WI, USA, 2009.

[71] G. M. Sheldrick, '*SHELXT* – Integrated space-group and crystal-structure determination', *Acta Crystallogr. Sect. A* **2015**, *71*, 3–8.

[72] G. M. Sheldrick, 'Crystal structure refinement with SHELXL', *Acta Crystallogr. Sect. C* **2015**, *71*, 3–8.

[73] D. Jayatilaka, D. J. Grimwood, 'Tonto: A Fortran Based Object-Oriented System for Quantum Chemistry and Crystallography', in 'Computational Science – ICCS 2003. Lecture Notes in Computer Science', Vol. 2660, Eds. P. M. A. Sloot, D. Abramson, A. V. Bogdanov, Y. E. Gorbachev, J. J. Dongarra, A. Y. Zomaya, Springer, Berlin, Heidelberg, 2003, pp. 142–151.

[74] L. A. Malaspina, A. Genoni, S. Grabowsky, '*lamaGOET*: an interface for quantum crystallography', *J. Appl. Crystallogr.* **2021**, *54*, 987–995.

[75] Gaussian 09, Revision D.01, M. J. Frisch, G. W. Trucks, H. B. Schlegel, G. E. Scuseria, M. A. Robb, J. R. Cheeseman, G. Scalmani, V. Barone, G. A. Petersson, H. Nakatsuji, X. Li, M. Caricato, A. Marenich, J. Bloino, B. G. Janesko, R. Gomperts, B. Mennucci, H. P. Hratchian, J. V. Ortiz, A. F. Izmaylov, J. L. Sonnenberg, D. Williams-Young, F. Ding, F. Lipparini, F. Egidi, J. Goings, B. Peng, A. Petrone, T. Henderson, D. Ranasinghe, V. G. Zakrzewski, J. Gao, N. Rega, G. Zheng, W. Liang, M. Hada, M. Ehara, K. Toyota, R. Fukuda, J. Hasegawa, M. Ishida, T. Nakajima, Y. Honda, O. Kitao, H. Nakai, T. Vreven, K. Throssell, J. A. Montgomery Jr., J. E. Peralta, F. Ogliaro, M. Bearpark, J. J. Heyd, E. Brothers, K. N. Kudin, V. N. Staroverov, T. Keith, R. Kobayashi, J. Normand, K. Raghavachari, A. Rendell, J. C. Burant, S. S. Iyengar, J. Tomasi, M. Cossi, J. M. Millam, M. Klene, C. Adamo, R. Cammi, J. W. Ochterski, R. L. Martin, K. Morokuma, O. Farkas, J. B. Foresman, D. J. Fox, Gaussian, Inc., Wallingford CT, 2016.

[76] P. R. Spackman, M. J. Turner, J. J. McKinnon, S. K. Wolff, D. J. Grimwood, D. Jayatilaka, M. A. Spackman, '*CrystalExplorer*: a program for Hirshfeld surface analysis, visualization and quantitative analysis of molecular crystals', *J. Appl. Crystallogr.* **2021**, *54*, 1006–1011.

[77] E. Hupf, F. Kleemiss, T. Borrmann, R. Pal, J. M. Krzeszczakowska, M. Woińska, D. Jayatilaka, A. Genoni, S. Grabowsky, 'The effects of experimentally obtained electron correlation and polarization on electron densities and exchange-correlation potentials', *J. Chem. Phys.* **2023**, *158*, 124103.

[78] A. Genoni, 'On the termination of the X-ray constrained wavefunction procedure: reformulation of the method for an unequivocal determination of λ', *Acta Crystallogr. Sect. A* **2022**, *78*, 302–308.

[79] K. Brandhorst, J. Grunenberg, 'Efficient computation of compliance matrices in redundant internal coordinates from Cartesian Hessians for nonstationary points', *J. Chem. Phys.* **2010**, *132*, 184101.

[80] E. D. Glendening, C. R. Landis, F. Weinhold, '*NBO 7.0*: New vistas in localized and delocalized chemical bonding theory', *J. Comput. Chem.* **2019**, *40*, 2234–2241.

[81] AIMAll, T. A. Keith, 'TK Gristmill Software', Overland Park KS, USA, aim.tkgristmill.com, 2016.

[82] T. Lu, F. Chen, 'Multiwfn: A multifunctional wavefunction analyzer', *J. Comput. Chem.* **2012**, *33*, 580–592.

[83] W. Humphrey, A. Dalke, K. Schulten, 'VMD: Visual molecular dynamics', *J. Mol. Graphics* **1996**, *14*, 33–38.

[84] M. Kohout, 'Program DGrid-5.0', Dresden, Germany, 2018.

[85] M. Kohout, 'Electron localizability indicator and bonding analysis with DGrid', Chapt. 4 in 'Complementary Bonding Analysis', Ed. S. Grabowsky, De Gruyter, 2021, pp. 75–112.